RSC Advances

PAPER

View Article Online
View Journal | View Issue

Cite this: *RSC Adv.*, 2025, **15**, 6663

Received 13th February 2025
Accepted 17th February 2025

DOI: 10.1039/d5ra01059d

rsc.li/rsc-advances

Dispersive Pd islands-deposited Au nanorods for *in situ* SERS monitoring of catalytic reaction†

Wenjing Lu,[ab] Yurui Jiang,[a] Xiaobin Yao, *[c] Yan Yu,[a] Wei Shen,[ad] Meng Yang,[abd] Xingjiu Huang [abd] and Xianghu Tang *[abd]

In this study, a bifunctional material with SERS effect and catalytic performance is fabricated in which dispersive Pd islands are deposited on the surface of gold nonorods (AuNR@Pd islands) with the confined modification of surface active sites of AuNRs using 5-iodo salicylic acid (5-ISA), which optimize the performance of bifunctional materials.

Understanding the structure–activity relationship at a molecular level and identifying the factors that govern the catalytic performance are key issues when new catalysts are developed, characterized, and introduced. SERS (surface-enhanced Raman scattering) can provide the fingerprint information of molecules from their vibrational transitions,[1–3] thus displays extraordinary application value in studying chemical reaction mechanism catalyzed by noble metal nanoparticles in recent years.[4–6] Noble metals such as Au and Ag are excellent SERS substrates,[7,8] Au nanorods (AuNRs) have attracted enormous attention due to their highly adjustable morphologies, unique anisotropic plasmonic properties, and widely adjustable plasmon wavelength.[9–11] Pd and Pt can catalyze a lot of chemical reactions, but they are poor SERS substrates because of the weak coupling between their free electrons and visible lights.[12–14] For all, it is difficult to achieve the desired activities for simultaneous SERS and catalysis using monometallic Ag, Au, Pd, or Pt nanocrystals.[15,16] One approach to integrating SERS and catalytic properties on a single nanocrystal is to deposit Pd or Pt onto Au or Ag nanocrystals, forming bimetallic nanocrystals with dual functionality, which have shown enormous potentials in catalytic investigations.[17,18] Therefore, the development of a bifunctional metal substrate for *in situ* SERS detection of catalytic reactions is attracting more and more attention. For example, Xie *et al.* used bifunctional Au@Ni_3FeO_x core-satellite superstructure as SERS substrate to monitor interfacial oxygen evolution reaction (OER) progress, and found direct spectroscopic evidence of intermediate O–O species.[19] Zhao *et al.* used a borrowing strategy to synthesize bifunctional Au@PtNi nanoparticles. *In situ* SERS coupled with rotating disk electrode (SERS-RDE) was described to provide information about the intermediates involved in the electrocatalytic hydrogenation of nitrobenzene on PtNi under ambient conditions.[20]

Core–shell structures are commonly used in bifunctional research.[21] However, it has been reported that the shape of shell greatly influence SERS and catalytic properties.[22,23] Inspired by this issue, herein, dispersive Pd islands-deposited AuNRs for in situ SERS monitoring of catalytic reaction was carried out (Fig. 1). Typically, AuNRs coated with different Pd shells have been successfully synthesized: one with dense Pd shell (Fig. 2d and e) and another with dispersive Pd islands (Fig. 2g and h), among which the later one present a better SERS-catalysis bifunctional performance by regulating surfactants in synthetic processes. Simply, 1 mM Pd precursor(H_2PdCl_4) was used to synthesize the AuNR@Pd islands. By changing the surfactants, AuNRs were capped with CTAB using seed growth method, while AuNR@Pd islands were prepared by capping the AuNRs using CTAB and 5-ISA to stabilize the AuNRs surface.[24,25] It is proposed that the 5-

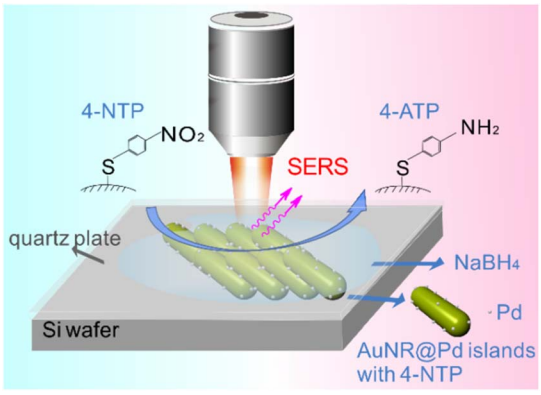

Fig. 1 Schematic illustration of *in situ* SERS monitoring of catalytic reaction.

[a]*Institute of Solid State Physics, HFIPS, Chinese Academy of Sciences, Hefei 230031, China. E-mail: tangxh2011@iim.ac.cn*

[b]*University of Science and Technology of China, Hefei 230026, China*

[c]*Department of Chemistry, The Hong Kong University of Science and Technology, Clear Water Bay, Hong Kong, China. E-mail: xiaobinyao@ust.hk*

[d]*Institute of Environmental Hefei Comprehensive National Science Center, Hefei, 230088, China*

† Electronic supplementary information (ESI) available. See DOI: https://doi.org/10.1039/d5ra01059d

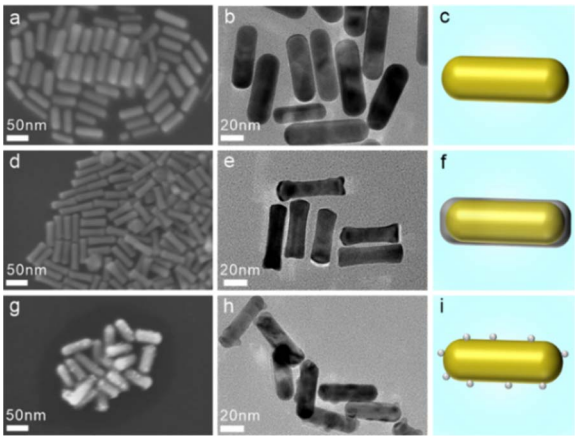

Fig. 2 SEM, TEM images and schematic diagram of (a–c) AuNRs; (d–f) AuNR@Pd shell; and (g–i) AuNR@Pd islands.

ISA interacts with the AuNRs surfactant bilayer with a cationic–π noncovalent interaction.[26] The surfactant bilayer on the AuNR surface becomes more packed upon the addition of 5-ISA,[27] and this slowed the nucleation rate of the Pd seeds on the surface of the AuNRs. Ascorbic acid (AA) and hydrochloric acid (HCl) were used as weak reducing agents,[28] which induced the Pd deposition on the surface of the AuNRs, and HCl helped to control the reduction rate.[29] Finally, AuNR@Pd shell with dense shell and AuNR@Pd islands with dispersive Pd islands were synthesized.

Initially, the structures and morphologies of the synthesized AuNR@Pd were characterized by using SEM and TEM. The SEM and TEM images clearly showed that AuNRs have an average size of 24 nm × 60 nm (Fig. 2a and b) and AuNR@Pd shell directly synthesized by using AuNRs capped with CTAB has a dense and smooth Pd shell (Fig. 2d and e). Notably, when CTAB was employed as a capping agent, H_2PdCl_4 should not be considered as the actual precursor. This was because a fast ligand-exchange reaction between $[PdCl_4]^{2-}$ and Br^- could occur and the major Pd^{2+} complex in the system would become $[PdBr_4]^{2-}$. Since the $[PdBr_4]^{2-}/Pd^0$ had a lower redox potential (~0.49 eV) *versus* $[PdCl_4]^{2-}/Pd^0$ (~0.62 eV),[30] the presence of Br^- ions led to a slower reduction rate of the Pd precursor, leading to a smooth Pd shell (~2 nm) (Fig. S1†). In comparison, due to the interaction between 5-ISA and CTAB, the surfactant layer of gold nanorods become more compact, which reduced the deposition rate of Pd, thus the AuNR@Pd islands had a bumpy surface with dispersive Pd islands(Fig. 2d, e and S2†).[31] UV-vis was used to investigate the structure and optical properties. As it can be clearly seen from Fig. S3,† after AuNRs were coated with different Pd nanostructures, the intensity of the longitudinal surface plasmon absorption peak decreases, and it has a slight red shift and further broadened. Corresponding element mapping Fig. 3a–c show that there were Pd and Au elements in the AuNR@Pd islands, and Pd islands were dispersive deposited on the AuNRs. Furthermore, X-ray photoelectron spectroscopy (XPS) was employed to analyze the surface composition and the oxidation state of the metals in the materials. The Pd 3d XPS spectra of AuNR@Pd islands in Fig. 3f

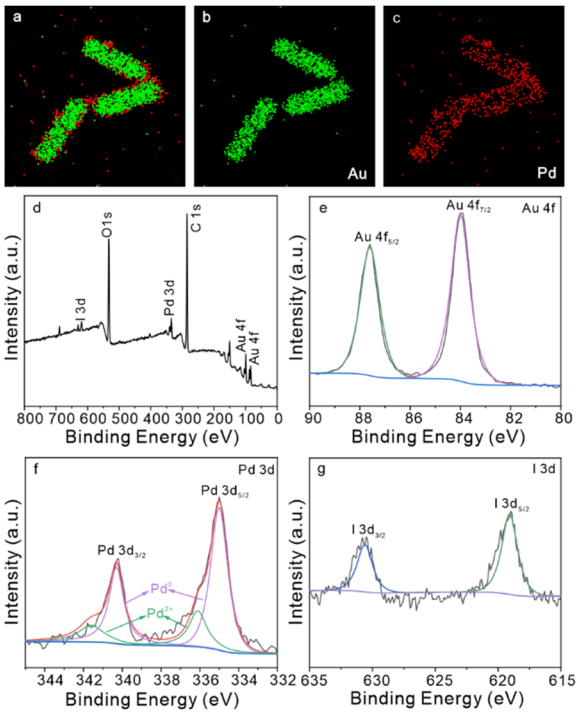

Fig. 3 (a–c) EDS mapping images of AuNR@Pd islands; (d–g) XPS spectra of AuNR@Pd islands – (d) the survey scan; (e) Au 4f; (f) Pd 3d; (g) I 3d.

showed that Pd^0 were mainly in their metallic states. The binding energies at 335.0 eV and 340.2 eV could be assigned to Pd $3d_{5/2}$ and Pd $3d_{3/2}$, respectively. Compared to the pure Pd metal (335.7 eV and 340.9 eV),[16,32] the binding energy of Pd 3d had a negative shifting, while the binding energy of Au 4f had a positive shifting, and the Pd^0 hold a dominant role. The peaks at 619.2 eV and 630.6 eV could be assigned to I $3d_{5/2}$ and I $3d_{3/2}$, corresponded to C–I covalent single bond in the 5-ISA. XPS spectra of AuNR@Pd Shell in Fig. S4† showed that, compared with the pure Au 4f (Au $4f_{5/2}$ 87.3 eV, Au $4f_{7/2}$ 83.5 eV),[33] the binding energy of Au 4f (Au $4f_{5/2}$ 87.7 eV, Au $4f_{7/2}$ 84.1 eV) shifted towards higher position, while the Pd 3d shifted towards lower position. This was mainly caused by the electron transfer from Au to Pd, which led to the change of the electronic structure of Au. All these obvious changes indicated the successful synthesis of AuNR@Pd islands and AuNR@Pd shell.

Subsequently, we used 10^{-7} M crystal violet (CV) molecules as a Raman probe to evaluate the SRES property of these two AuNR@Pd materials (Fig. 4). Obviously, the SERS signal intensity collected under the naked AuNRs substrate was significantly higher than those of other AuNRs deposited by Pd. It was suggested that the deposition of Pd atoms on AuNRs would deteriorate their SERS activity.[34] More importantly, the SERS signal intensity collected under AuNR@Pd islands was higher than AuNR@Pd shell. It was assumed that such a decrease may also arise from the Pd shell reducing the direct contact between CV and AuNRs surface. Additionally, AuNR@Pd islands had a bumpy surface with dispersive Pd islands may expose more

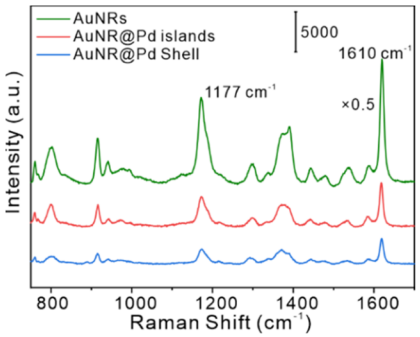

Fig. 4 SERS spectra of CV acquired from different substrates.

surface of gold nanorods to enhance the SERS performance and possessed an acceptable SERS enhancement ability.

Next, the catalytic activity of AuNR@Pd was evaluated by using the model reduction of 4-NTP to 4-aminothiophenol (4-ATP).[35] Typically, UV-vis spectroscopy was used to monitor the decay of the adsorption peak of 4-NTP at 400 nm as reduction proceeded after adding catalyst. Fig. 5b showed the absorption spectra of 4-NTP as a function of time which indicated the reduction of 4-NTP catalyzed by AuNR@Pd islands with $NaBH_4$ solution. After the $NaBH_4$ was added, the ionization of 4-NTP took place in alkaline solution,[36] a strong UV-vis absorption peak of 4-NTP at 400 nm could be clearly observed from the Fig. 5b (black line). The position and intensity of the maximum absorption peak did not change with time, indicating that individual $NaBH_4$ is unable to reduce 4-NTP (Fig. S5†). While after the AuNRs were added into the solution (as shown in Fig. S6†), within 180 min, the intensities and positions of the UV-vis spectra did not change significantly, indicating that AuNRs basically did not have catalytic performance. The spectra Fig. 5b confirmed that the Pd deposited on the AuNRs could accelerate the reduction. With the addition of AuNR@Pd islands, the intensity of the UV-vis absorption peak at 400 nm gradually decreased, at ~18 min (green curve), there was a new UV-vis absorption peak at 300 nm appeared, this was the typical characteristic peak of 4-ATP, which represented that the 4-NTP was reduced to 4-ATP. In the system, the concentration of 4-NTP was lower and lower, and the concentration of 4-ATP was gradually increased. At ~25 min, the characteristic absorption peak of 4-NTP disappeared completely indicating the end of reaction and the color of solution changed from yellow to colorless. In contrast, it was noted that AuNR@Pd shell did not show comparable catalytic effects. While added AuNR@Pd shell (as shown in Fig. S7†), UV-vis spectra did not have any apparent change until 35 min. It showed that these AuNR@Pd with Pd deposited on the surfaces could accelerate the reaction, and the catalytic performance of AuNR@Pd shell with dense and smooth Pd shell was not good as that of AuNR@Pd islands with dispersive Pd. It was assumed that AuNR@Pd islands with dispersive Pd can expose more active sites for the reaction. Therefore, the construction of AuNR@Pd islands is a much better candidate of bifunctional materials. Furthermore, to check the influence of the amounts of Pd islands to catalyze reactions, 4 types of AuNR@Pd islands were checked by adjusting the volume of H_2PdCl_4 (Table S1†). The UV-vis of 4-NTP reduction catalyzed by different AuNR@Pd islands were shown in Fig. S8–S10.† Clearly, with the decrease of Pd islands, the catalytic performance of AuNR@Pd islands was quickly weakened, consistent with the calculated first-order kinetic constant of the reaction (Table S2†). Fig. S12† shows the absorption at 400 nm as a function of reaction time in the presence of different AuNR@Pd islands. Oppositely, the SERS effect increased with the decreasing of Pd islands (Fig. S11 and S13†).

To realize the aim of fabricating a bifunctional substrate and benefit with the high sensitivity of SERS, the AuNR@Pd islands1 with the best catalytic activity and an acceptable SERS enhancement ability were selected for *in situ* SERS monitoring of the reduction of 4-NTP. Firstly, 4-NTP molecules were incubated with AuNR@Pd islands1 for 12 h. After centrifugation, they were dropped on silicon wafers and dried at room temperature. Then $NaBH_4$ solution was added dropwise to start the catalytic reaction. At the same time, an ultra-thin quartz sheet was quickly covered to avoid evaporation of the liquid. By collecting SERS signals, the catalytic reduction reaction of 4-NTP was dynamically monitored *in situ*. At $t = 0$, Fig. 6 showed the SERS spectrum of 4-NTP with three characteristic vibrational bands at 1108 cm^{-1}, 1326 cm^{-1}, and 1569 cm^{-1}. As the

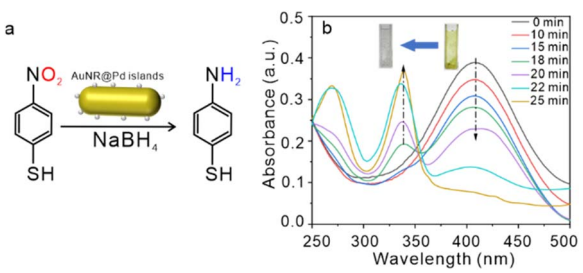

Fig. 5 (a) Reaction scheme for the conversion of 4-NTP to 4-ATP in the presence of NaBH4 and AuNR@Pd islands; (b) UV-vis of 4-NTP reduction catalyzed by AuNR@Pd islands.

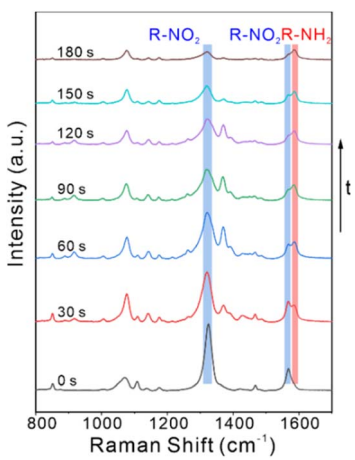

Fig. 6 Time-dependent SERS spectra of recorded during the reduction of 4-NTP to 4-ATP catalyzed by AuNR@Pd islands1.

reaction proceeded, the intensity of these bands decreased gradually, and a new band emerged corresponding to the phenol-ring mode of 4-ATP at 1590 cm^{-1} (red block), the other vibrational modes shown in the SERS spectra can also be assigned to those shown in Raman spectra of 4-NTP and 4-ATP (Table S3†), which realized *in situ* SERS real-time monitoring of 4-NTP to 4-ATP catalytic reduction. Hence, we demonstrated that the AuNR@Pd islands1 are capable of SERS and catalytic activity.

In summary, dispersive Pd islands were deposited onto AuNRs (*i.e.*, AuNR@Pd islands) by regulating the surfactants of CTAB and 5-ISA which showed different morphologies from AuNRs with dense Pd shells (*i.e.*, AuNR@Pd shell) regulated by a sole surfactant of CTAB. It was assumed that ISA competitively interacted with CTAB and finally induced the formation of dispersive Pd islands. More importantly, compared with the AuNR@Pd Shell, AuNR@Pd islands presented better bifunctional performance of SERS and catalytic activity on the catalytic reduction of 4-NTP to 4-ATP. This AuNR@Pd islands substrate and the corresponding strategy shows the significance of regulating the bifunctional substrate for simultaneous *in situ* SERS and catalytic investigation of environment, energy, catalysis, *etc*.

Data availability

The data supporting this article have been included as part of the ESI.†

Conflicts of interest

There are no conflicts to declare.

Acknowledgements

This work was supported by the National Natural Science Foundation of China (No. 22204166), the National Key R&D Program of China (No. 2021YFB3201400), The Youth Innovation Promotion Association of CAS (No. 2023469), the Key R&D Program of Anhui Province (No. 202104i07020011), the HFIPS Director's Fund (No. YZJJ202102, No. YZJJ-GGZX-2022-01).

Notes and references

1 R. Peng, T. T. Zhang, S. Yan, Y. X. Song, X. Y. Liu and J. S. Wang, *Nanomaterials*, 2023, **13**, 28.
2 X. X. Han, R. S. Rodriguez, C. L. Haynes, Y. Ozaki and B. Zhao, *Nat. Rev. Methods Primers*, 2022, **1**, 87.
3 X. L. Zheng, Z. W. Ye, Z. Akmal, C. He, J. L. Zhang and L. Z. Wang, *Chem. Soc. Rev.*, 2024, **53**, 656–683.
4 J. Langer, D. Jimenez de Aberasturi, J. Aizpurua, R. A. Alvarez-Puebla, B. Auguie, J. J. Baumberg, G. C. Bazan, S. E. J. Bell, A. Boisen, A. G. Brolo, J. Choo, D. Cialla-May, V. Deckert, L. Fabris, K. Faulds, F. J. Garcia de Abajo, R. Goodacre, D. Graham, A. J. Haes, C. L. Haynes, C. Huck, T. Itoh, M. Kall, J. Kneipp, N. A. Kotov, H. Kuang, E. C. Le Ru, H. K. Lee, J. F. Li, X. Y. Ling, S. A. Maier, T. Mayerhofer, M. Moskovits, K. Murakoshi, J. M. Nam, S. Nie, Y. Ozaki, I. Pastoriza-Santos, J. Perez-Juste, J. Popp, A. Pucci, S. Reich, B. Ren, G. C. Schatz, T. Shegai, S. Schlucker, L. L. Tay, K. G. Thomas, Z. Q. Tian, R. P. Van Duyne, T. Vo-Dinh, Y. Wang, K. A. Willets, C. Xu, H. Xu, Y. Xu, Y. S. Yamamoto, B. Zhao and L. M. Liz-Marzan, *ACS Nano*, 2020, **14**, 28–117.
5 H.-L. Zhong, H. Ze, X.-G. Zhang, H. Zhang, J.-C. Dong, T. Shen, Y.-J. Zhang, J.-J. Sun and J.-F. Li, *ACS Catal.*, 2023, **13**, 6781–6786.
6 D. Wang, F. X. Shi, J. Jose, Y. F. Hu, C. N. Zhang, A. N. Zhu, R. Grzeschik, S. Schlücker and W. Xie, *J. Am. Chem. Soc.*, 2022, **144**, 5003–5009.
7 M. J. Oh, S. Kwon, S. Lee, I. Jung and S. Park, *ACS Nano*, 2024, **18**, 7656–7665.
8 A. Brancato, M. Condorelli, L. Salemi, V. Scardaci, M. Fragal, M. Barcellona, G. Compagnini and L. D'Urso, *Surface. Interfac.*, 2023, **40**, 103157.
9 J. P. Zheng, X. Z. Cheng, H. Zhang, X. P. Bai, R. Q. Ai, L. Shao and J. F. Wang, *Chem. Rev.*, 2021, **121**, 13342–13453.
10 Y. A. Xia, Q. Chen and U. Banin, *Chem. Rev.*, 2023, **123**, 3325–3328.
11 G. M. Das, S. Manago, M. Mangini and A. C. De Luca, *Nanomaterials*, 2021, **11**, 24.
12 Z. Q. Tian, B. Ren, J. F. Li and Z. L. Yang, *Chem. Commun.*, 2007, 3514–3534.
13 H. J. Ze, X. Chen, X. T. Wang, Y. H. Wang, Q. Q. Chen, J. S. Lin, Y. J. Zhang, X. G. Zhang, Z. Q. Tian and J. F. Li, *J. Am. Chem. Soc.*, 2021, **143**, 1318–1322.
14 L. Yang, R. Grzeschik, P. Jiang, L. F. Yu, C. J. Hu, A. X. Du, S. Schluecker and W. Xie, *Angew. Chem. Int. Ed.*, 2023, **62**, 5.
15 C. C. Zhang, Y. L. Li, A. A. Zhu, L. Yang, X. M. Du, Y. F. Hu, X. Yang, F. Zhang and W. Xie, *Chin. Chem. Lett.*, 2023, **34**, 4.
16 J. Wei, Y. J. Zhang, S. N. Qin, W. M. Yang, H. Zhang, Z. L. Yang, Z. Q. Tian and J. F. Li, *Chem. Commun.*, 2019, **55**, 8824–8827.
17 Y. L. Sun, A. Yao-Lin, M. F. Yue, H. Q. Chen, H. J. Ze, Y. H. Wang, J. C. Dong, Z. Q. Tian, P. P. Fang and J. F. Li, *Anal. Chem.*, 2022, **94**, 4779–4786.
18 X. Zhou, H. Q. Huang, Y. Q. Yang, H. L. Zhou, R. Y. Liang, Y. J. Zhao, Q. Y. Cui, Y. H. Tang, S. Y. Chen, P. Li, H. H. Cai, P. H. Sun, W. P. Xu, W. Y. Yang and H. B. Zhou, *Sens. Actuators, B*, 2023, **394**, 134385.
19 C. J. Hu, Y. F. Hu, C. H. Fan, L. Yang, Y. T. Zhang, H. X. Li and W. Xie, *Angew. Chem. Int. Ed.*, 2021, **60**, 19774–19778.
20 J. Ma, Z. Wang, T. Majima and G. Zhao, *ACS Catal.*, 2022, **12**, 14062–14071.
21 Z. Yong, Q. Shi, R. Fu and W. Cheng, *Adv. Mater. Interfaces*, 2021, **8**, 2001686.
22 T. Guo, M. M. Murshed, K. Rezwan and M. Maas, *Adv. Mater. Interfaces*, 2023, **10**, 2300207.
23 Q. Zhang, T.-S. Deng, Y.-Q. Dou, M.-Z. Wei, S. Li, J. Liu and Z. Cheng, *ACS Appl. Nano Mater.*, 2022, **5**, 17048–17058.
24 L. Scarabelli, M. Grzelczak and L. M. Liz-Marzán, *Chem. Mater.*, 2013, **25**, 4232–4238.
25 M. I. Firmanti and J. W. Ha, *J. Phys. Chem. Lett.*, 2023, **14**, 8016–8023.

26 Y. H. Zhan, D. Y. Lei, X. F. Li and S. A. Maier, *Nanoscale*, 2014, **6**, 4705–4715.
27 N. Ortiz, S. J. Hong, F. Fonseca, Y. Liu and G. Wang, *J. Phys. Chem. C*, 2017, **121**, 1876–1883.
28 S. X. Bao, X. Yang, M. Luo, S. Zhou, X. Wang, Z. X. Xie and Y. N. Xia, *Chem. Commun.*, 2016, **52**, 12594–12597.
29 M. Z. Wei, T. S. Deng, Q. Zhang, Z. Q. Cheng and S. Q. Li, *ACS Omega*, 2021, **6**, 9188–9195.
30 M. H. Xie, S. Zhou, J. W. Zhu, Z. H. Lyu, R. H. Chen and Y. N. Xia, *Chem. Eur J.*, 2019, **25**, 16397–16404.
31 X. C. Zhou, Y. B. Ma, Y. Y. Ge, S. Q. Zhu, Y. Cui, B. Chen, L. W. Liao, Q. B. Yun, Z. He, H. W. Long, L. J. Li, B. A. Huang, Q. X. Luo, L. Zhai, X. X. Wang, L. C. Bai, G. Wang, Z. Q. Guan, Y. Chen, C. S. Lee, J. L. Wang, C. Y. Ling, M. H. Shao, Z. X. Fan and H. Zhang, *J. Am. Chem. Soc.*, 2022, **144**, 547–555.
32 S. Yang, Q. Li, C. Li, T. L. Cao, T. Q. Wang, F. Q. Fan, X. M. Zhang and Y. Fu, *ACS Appl. Mater. Interfaces*, 2021, **13**, 52754–52764.
33 C. Li, H. L. Zhu, Y. Guo, S. S. Ye, T. Q. Wang, Y. Fu and X. M. Zhang, *ACS Sens.*, 2022, **7**, 2778–2787.
34 J. M. Li, J. Y. Liu, Y. Yang and D. Qin, *J. Am. Chem. Soc.*, 2015, **137**, 7039–7042.
35 Y. Zhang, Y. R. Wu and D. Qin, *J. Mater. Chem. C*, 2018, **6**, 5353–5362.
36 Q. Dai, J. Huang, X. Qiu, N. Wang, D. Wang and Y. Li, *J. Alloys Compd.*, 2024, **1005**, 176018.